Communication

Journal of Photopolymer Science and Technology
Volume 33, Number 2 (2020) 153 – 158 ©2020SPST

Photon-induced Fragmentation of Zinc-based Oxoclusters for EUV Lithography Applications

Neha Thakur[1], Alexandre Giuliani[2,3], Laurent Nahon[2], and Sonia Castellanos[1*]

[1]Advanced Research Center for Nanolithography, Science Park 106, 1098XG Amsterdam, the Netherlands
[2]Synchrotron SOLEIL, l'Orme des Merisiers, St Aubin, BP48, 91192 Gif sur Yvette Cedex, France
[3] INRAE, UAR1008, Transform Department, Rue de la Géraudière,
BP 71627, 44316 Nantes, France
**s.castellanos@arcnl.nl*

To meet the requirements for EUV nanolithography, the semiconductor industry has drawn attention towards hybrid inorganic-organic based photoresists. However, the mechanisms responsible for the solubility switch in these materials are not well understood. In this work, UV/ VUV (4-14 eV) photon-induced fragmentations of Zn-based oxoclusters in the gas phase are investigated to study the fundamental reactivity of their cationic form. Irradiation of the parent cations results mainly in the ligand dissociation and fragmentation of the inorganic clusters at energies below the second ionization threshold (~12 eV). This ionization energy appears to be linked to the methacrylate ligand in the organic shell. We presume that this type of fragmentations can also occur when the oxoclusters are ionized in the thin film upon EUV irradiation.

Keywords: Photoresist, Hybrid material, Photochemistry, Mass spectrometry

1. Introduction

As the lithography technology shifted from 193 nm (Deep Ultraviolet, DUV) towards a shorter wavelength of 13.5 nm (Extreme Ultraviolet, EUV), metal-based resist systems emerged as a promising alternative to the traditional organic chemically amplified resists (CARs) [1-4]. This unprecedented growing interest in metal-based resists systems is due to one key contribution of the metals in the lithographic process: the enhancement of the projected image absorption by the resist [5-8]. This is because the absorption cross-section of EUV photons is generally higher for metals as compared to C, H, O, N, which are constituting elements of organic CARs.

Metal-oxo clusters (MOCs), a class of hybrid inorganic-organic molecular material, have emerged as promising photoresists for EUV lithography (EUVL) applications. MOCs have a molecularly defined small structure and offer synthetic versatility, as they can undergo ligand-exchange reactions [9-11]. In previous published studies by some of the authors, Zn-MOCs, $Zn_4O(MA)_{6-x}(TFA)_x$ having a mixed organic shell containing both methacrylate (MA) and trifluoroacetate (TFA) ligands has shown high sensitivity/ reactivity towards EUV photons and good EUVL performance [12]. The experimental absorption coefficient of Zn-MOCs is also relatively high (12.4 μm^{-1}) as compared to traditional photoresist (5 μm^{-1}). However, the mechanism behind the solubility switch upon exposure to such high energy EUV radiation is not yet well established for resist materials, in general, and for this novel Zn-MOCs resist, in particular [2,13,14]. Thus, the reaction paths triggered by EUV-irradiation on inorganic resists that enable patterning in lithography is currently a very active research area. EUV photons (13.5 nm, 92 eV) exceed the ionization potential of the photoresist material (~10 eV) such that exposure to EUV results in the ionization of the material. The ionization is accompanied by the emission of a photoelectron with up to 80 eV energy that is capable to trigger an electron cascade, i.e. the formation of several secondary electrons and holes [15-18].

The study at molecular level of the complex reaction mechanisms and of the resultant chemical

Received March 11, 2020
Accepted March 16, 2020

changes occurring in resists' thin films (tenths of nanometers thickness) upon EUV exposure is challenging [19]. Alternatively, the reactivity of metal-oxoclusters can be studied in the gas phase. This method has been utilized previously to study the decay paths that an excited MOC can undergo and how these paths can differ when different organic ligands are used [20,21].

In this work, we studied photon-induced fragmentation of Zinc-based MOCs, $Zn_4O(MA)_{6-x}(TFA)_x$. Zn-MOCs were brought into the gaseous phase in their cationic form (with a net charge of +1), trapped and exposed to ultraviolet (UV) and vacuum ultraviolet (VUV) radiation (4-14 eV range). The resultant photon-induced fragments and ionization products were identified with a mass spectrometer coupled to the ion trap. These experiments reveal the reactions that the ionized Zn-based photoresist molecules undergo and give us insights into the possible species that can derive from the holes formed in the thin film upon EUV exposure.

2. Experimental

To perform the photo-induced fragmentation experiments, a solution of $Zn_4O(MA)_{6-x}(TFA)_x$ was prepared (1.5 mg in 1 mL of an acetonitrile/acetone mixture in 3:2 ratio, 4 min sonication) and filtered. A commercial linear quadrupolar ion trap (Thermo Scientific LTQ XL) mass spectrometer using atmospheric pressure photoionization (APPI) source coupled to the DESIRS beamline at SOLEIL synchrotron radiation facility (France) was used [22,23]. A syringe pump with a flow rate of 10 µL min^{-1} was used for all the experiments. The molecules were ionized by the Krypton discharge lamp of the APPI source. The parent cations were selectively trapped in the linear quadrupole ion trap and exposed to monochromatic and high-harmonics free (by using Kr-filled gas filter and a quartz window when required) photons. The curves were normalized to the photon flux variations over energy range 4-14 eV (measured by using a Si photodiode) to obtain relative cross section or photon-normalized ion yield. DFT calculations were performed with Gaussian 16 [24] using the functional UB3LYP and the Def2TZVP basis set.

3. Results and discussion

The $Zn_4O(MA)_{6-x}(TFA)_x$ (x= 0 or 1) MOCs studied in this work have 4 Zn atoms in a tetrahedral geometry bridged by an O in center (μ_4-oxo) in their inorganic core. They were synthesized by a ligand exchange method as previously reported [12] using $Zn_4O(TFA)_6$ as a precursor, which has the same oxo-core and 6 TFA ligands in the organic shell. TFA ligands were exchanged by MA ligands (a ligand of interest for nanolithography applications) [2,11,12,25]. This reaction proceeds in an equilibrium and therefore, the composition of the resulting Zn-MOCs have a statistical distribution of the combination of both MA and TFA ligands in the organic shell, where MA is the more abundant ligand. Through our previous analytical spectroscopy studies, we deduced that the synthesized Zn-MOCs have on average a MA/TFA ratio of approximately 5:1, i.e. the average formula is close to $Zn_4O(MA)_5(TFA)$ [12].

To generate the parent ion species from the neutral Zn-oxoclusters, APPI was used. Figure 1. displays the mass spectra of the four trapped parent ions before irradiation. As expected from the statistical distribution in the ligand composition, two of the trapped parent ions were identified as: 1) the product of ionization of the Zn-MOC with a 5:1 MA/TFA ratio at *m/z* 816.05, labeled as $[P_1]^{\bullet+}$= $[Zn_4O(MA)_5(TFA)]^{\bullet+}$; 2) its analogue with all 6 MA ligands at *m/z* 788.12, $[P_2]^{\bullet+}$= $[Zn_4O(MA)_6]^{\bullet+}$. The ability to isolate the parent with 5:1 MA/TFA ligands and the parent with all 6 MA ligands allowed us to study the influence of the TFA ligand on the reactivity of the radical cation of the Zn-MOCs.

In addition, the ions that result from one ligand loss from the starting neutral molecules $[P_1\text{-}L_1]^+$ = $[Zn_4O(MA)_4(TFA)]^+$, *m/z* 730.97. $[P_1\text{-}L_2]^+$ = $[P_2\text{-}L_1]^+$ = $[Zn_4O(MA)_5]^+$, *m/z* 703.04, where L_1 = MA and L_2 = TFA, could also be trapped. However, in the latter cases the trapping always led to the co-existence of the hydrated species $[P_1\text{-}L_1\text{+}H_2O]^+$ and $[P_2\text{-}L_1\text{+}H_2O]^+$ = $[P_1\text{-}L_2\text{+}H_2O]^+$, which might result from the hygroscopic nature of the Zn-based inorganic core.

The simulated isotopic distribution (shown in blue using online tool Chemcal [26]) in Fig. 1. remains the same for all the clusters (at the corresponding *m/z* values), regardless of the presence of 5 or 6 ligands in their organic shell. This is because this pattern results from the 4 Zn atoms and is thus a fingerprint of the tetranuclear inorganic cluster. A broadening of the peaks was observed for $[P_{1/2}\text{-}L_{1/2}\text{+}H_2O]^+$ adducts. The origin of this feature is unclear and needs further investigations that are out of the scope of this work.

As an example of the photo-fragmentation products formed from the different parent ions, the

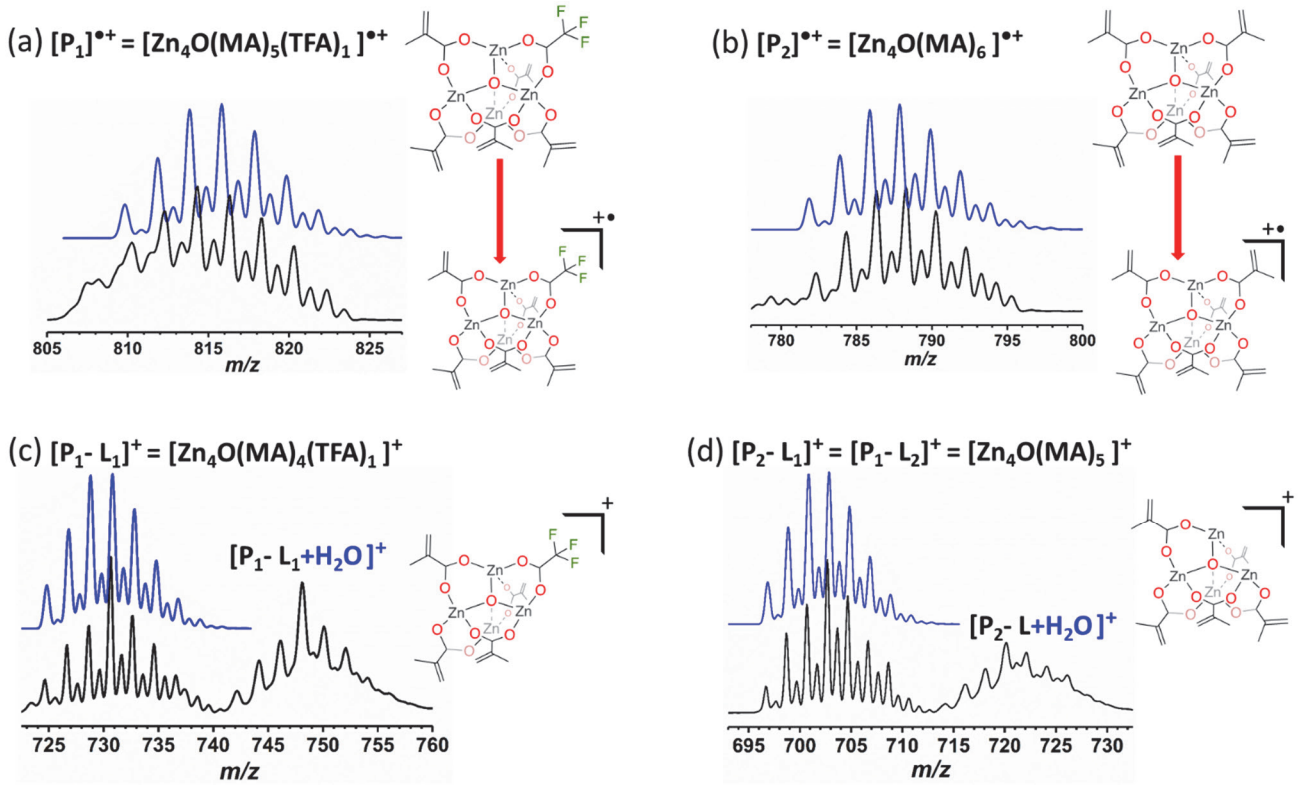

Fig. 1. Mass spectra of the four trapped parent ions before irradiation. Simulated isotopic distribution is shown in blue.

mass spectra acquired after irradiation of $[P_1]^{\bullet+}$ and $[P_1\text{-}L_1]^+$ at 13.5 eV photons energy is shown in Fig. 2. The counterparts derived from $[P_2]^{\bullet+}$ and $[P_2\text{-}L_1]^+$ (=$[P_1\text{-}L_2]^+$) yielded analogous results and are not shown for simplicity. At this energy, the second ionization products of all parent ions were detected. For parent ions identified as $[P_{1/2}]^{\bullet+}$, with 6 ligands, the double charged ions, labeled as $[P_{1/2}]^{2+}$, were accompanied by the adducts resulting from the coordination of one or two water molecules, $[P_{1/2}+xH_2O]^{2+}$, x=1-2, whereas in the case of the doubled charged species with 5 ligands, only the hydrated adducts, $[P_1\text{-}L_{1/2}+xH_2O]^{2\bullet+}$, x=1-3, were observed (insets in Fig. 2).

Noticeably, a product identified as $[Zn_3O(MA)_3]^+$ was detected at *m/z* 467.46 in the spectra of all the irradiated parent ions. The isotopic mass distribution clearly matched the presence of only 3 Zn atoms (Fig. 3). The formation of this species reveals that the inorganic cluster can dissociate such that one Zn atom can detach from the molecule.

In the particular case of the parent ions $[P_{1/2}]^{\bullet+}$, the product of ligand dissociation $[P_{1/2}\text{-}L_1]^+$ and its adduct with acetonitrile, $[P_{1/2}\text{-}L_1+CH_3CN]^+$ was observed at a lower energy (Fig. 4. shown at 9 eV). Furthermore, in this *m/z* range, species that match the molecular weight of $[P_{1/2}\text{-}OH]^+$ was detected. We hypothesize that protonation of the μ_4-oxo group might open this reaction path.

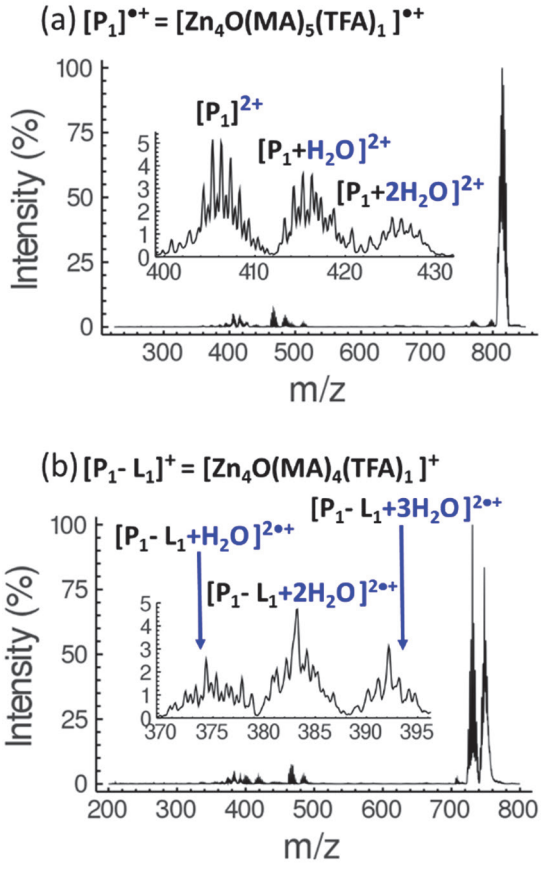

Fig. 2. Mass spectra after irradiation with 13.5 eV photons. Zoomed in regions shows the second ionization products accompanied by water adducts.

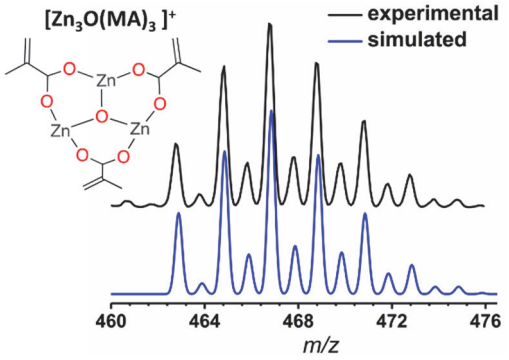

Fig. 3. Observed and simulated (blue) mass distribution of $[Zn_3O(MA)_3]^+$ as a photo- fragmentation product, from all four parent species.

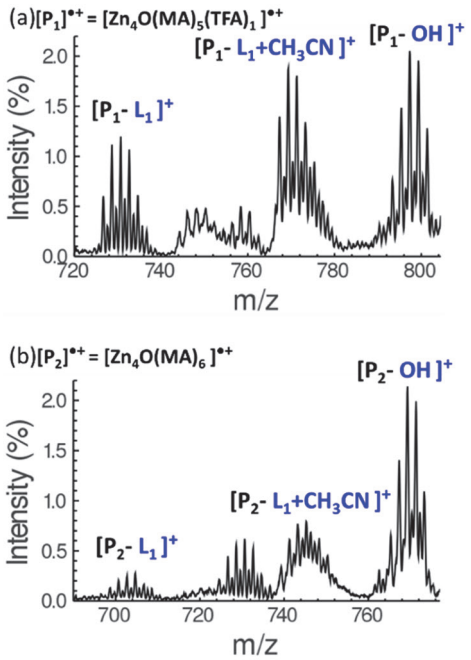

Fig. 4. Ligand dissociation products, $[P_{1/2}\text{-}L_1]^+$ and product assigned to OH loss observed after irradiation with 9 eV photons of the parent ions $[P_{1/2}]^{\bullet+}$.

The relative yields of photo-products are plotted as a function of photon energy in Fig. 5. (4-7.4 eV) and Fig. 6. (7-14 eV). Photo-fragments in the lower energy range were only detected for the parent ions, $[P_{1/2}]^{\bullet+}$, with 6 carboxylate ligands, shown in Fig. 5.

Ligand dissociation products were predominant in the energy range of 7-14 eV for the $[P_{1/2}]^{\bullet+}$ parent ions, as shown in Figs. 6(a) and (b). Yet, for all the four parent ions, also the ones with 5 ligands only ($[P_{1/2}\text{-}L_1]^+$), the Zn-trinuclear species $[Zn_3O(MA)_3]^+$ forms above 7-8 eV. In the case of $[P_1]^{\bullet+}$, the analogue of $[Zn_3O(MA)_3]^+$ species $[Zn_3O(MA)_2(TFA)]^+$ was also detected. The proposed photo-fragmentation reactions for all four parent ions combined are shown in Scheme 1. We presume that when more than one ligand is lost, the inorganic core is destabilized, as one Zn atom in the tetranuclear structure is left with only one bridging carboxylate ligand. Thus, the tetranuclear cluster has an excess of positive charge. Therefore, one Zn atom is lost, along with a ligand. This is why $[P\text{-}MA]^+$ type, or $[P\text{-}OH]^+$ products are not seen in Figs. 6(c) and (d).

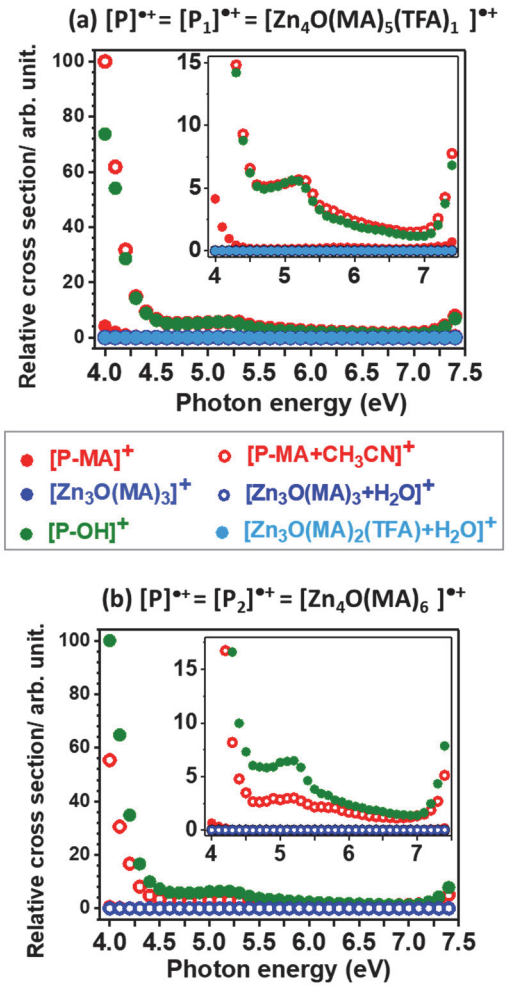

Fig. 5. Photon normalized yield of the products formed in the 4-7.4 eV photon range from $[P_{1/2}]^{\bullet+}$.

The onset of the second photo-ionization for all parent ions and related adducts with solvent molecules is observed around 12 eV. This result suggests that the ionization energy of the parent ions is determined by the molecular orbitals on the MA ligand. Indeed, the ionization potential estimated with DFT calculations for parent ions $[P_1]^{\bullet+}$ and $[P_2]^{\bullet+}$ are 11.4 eV and 11.1 eV, respectively and the highest occupied orbital for both radical cations is mainly located on the MA unit (Fig. 7). Interestingly, the di-cation preserved the molecular structure with all ligands and seemed to have high affinity towards water molecules.

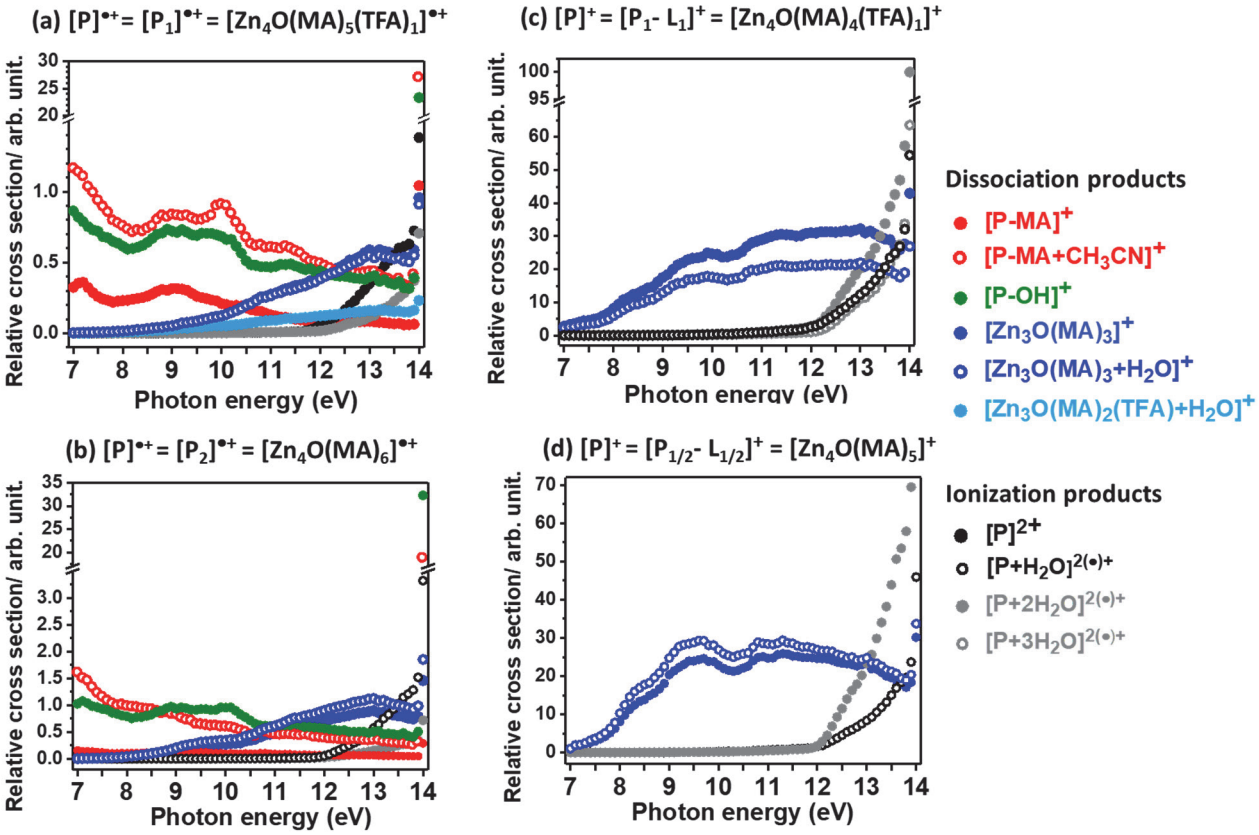

Fig. 6. Photon-normalized ion yield of the products formed from their respective parent ions.

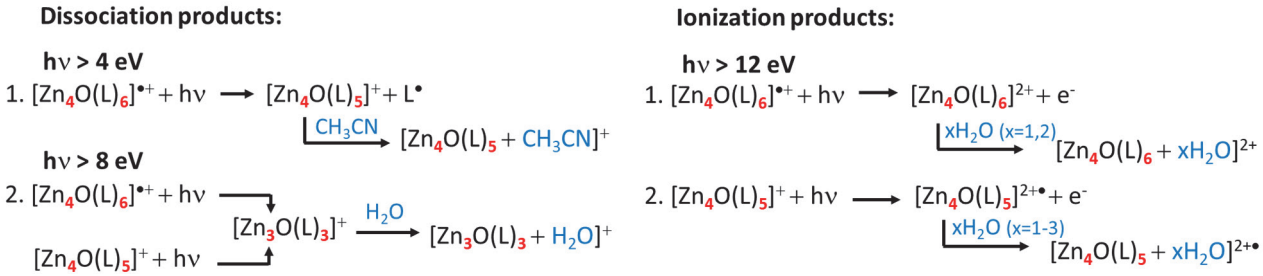

Scheme 1. Proposed photo-fragmentation reactions of the parent ions.

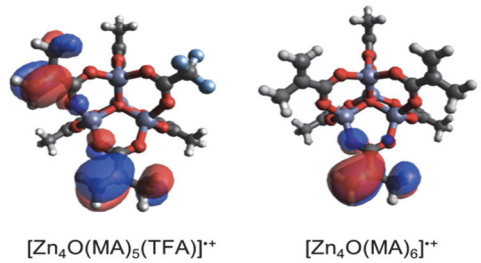

Fig. 7. Highest occupied molecular orbitals (HOMO) of parent ions $[P_1]^{\bullet+}$ and $[P_2]^{\bullet+}$ calculated with DFT (UB3LYP, Def2TZVP).

4. Conclusions

Photo-induced fragmentations studies on the mixed ligand Zn-MOCs, $Zn_4O(MA)_{6-x}(TFA)_x$, exposed to UV/VUV (4 to 14 eV) photons in the gas phase helps to identify the most favorable reaction pathways that this molecular EUV resist follows when is ionized and brought to different excited states. Ligand dissociation proved to be a main reaction path at energies below the second ionization energy threshold (~12 eV) for the parent ionic species $[P_{1/2}]^{\bullet+}$. However, further ligand dissociations seem to lead to the dissociation of the inorganic core and loss of one Zn atom. Above ~12 eV, second photo-ionization processes compete with the photo-fragmentation ones, which indicates that the energy is used for the emission of an electron rather than for bond dissociation. The presence of the TFA ligand in the organic shell does not seem to influence in the photoionization energy, compatible with HOMO orbitals localized on the MA ligand(s). Despite the fact that EUV energy is higher than the range of energy used in this study, this work gives

fundamental insights into the reactive sites and the stability of the cationic species of $Zn_4O(MA)_{6-x}(TFA)_x$, which can be formed in thin films upon exposure to the ionizing EUV radiation.

Acknowledgements

The authors acknowledge the contribution of Alessandro Antoncecchi for his help with data plotting. We thank the whole SOLEIL staff for running the facility under project 20190813. This work was supported by the Agence Nationale de la Recherche (France), under project number ANR-08-BLAN-0065.

References

1. L. Li, X. Liu, S. Pal, S. Wang, C. K. Ober, and E. P. Giannelis, *Chem. Soc. Rev.*, **46** (2017) 4855.
2. L. Wu, M. Baljozovic, G. Portale, D. Kazazis, M. Vockenhuber, T. Jung, Y. Ekinci, and S. Castellanos, *J. Micro/Nanolith. MEMS MOEMS*, **18** (2019) 13504.
3. A. Lio, *Proc. SPIE*, **9776** (2016) 97760V.
4. N. Mark, K. Cho, and K. Petrillo, *J. Photopolym. Sci. Technol.*, **25** (2012) 87.
5. R. Fallica, J. Haitjema, L. Wu, S. C. Ortega, A. M. Brouwer, and Y. Ekinci, *J. Micro/Nanolith. MEMS MOEMS*, **17** (2018) 23505.
6. T. Kozawa and S. Tagawa, *Jpn. J. Appl. Phys.*, **47** (2008) 8354.
7. R. Fallica, J. K. Stowers, A. Grenville, A. Frommhold, A. P. G. Robinson, and Y. Ekinci, *J. Micro/Nanolith. MEMS MOEMS*, **15** (2016) 33506.
8. X. Wang, Z. Tasdemir, I. Mochi, M. Vockenhuber, L. van Lent-Protasova, M. Meeuwissen, R. Custers, G. Rispens, R. Hoefnagels, and Y. Ekinci, *Proc. SPIE*, **10957** (2019) 109570A.
9. P. Walther, M. Puchberger, F. R. Kogler, K. Schwarz, and U. Schubert, *Phys. Chem. Chem. Phys.*, **11** (2009) 3640.
10. J. Kreutzer, M. Puchberger, C. Artner, and U. Schubert, *Eur. J. Inorg. Chem.*, **2015** (2015) 2145.
11. L. Wu, M. Vockenhuber, Y. Ekinci, and S. Castellanos, *Proc. SPIE*, **10957** (2019) 109570B.
12. N. Thakur, L.-T. Tseng, M. Vockenhuber, Y. Ekinci, and S. Castellanos, *J. Micro/Nanolith. MEMS MOEMS*, **18** (2019) 43504.
13. I. Pollentier, Y. Vesters, J. Jiang, P. Vanelderen, and D. de Simone, *Proc. SPIE*, **10450** (2017) 104500H.
14. H. Fukuda, *J. Micro/Nanolith. MEMS MOEMS*, **18** (2019) 13503.
15. Y. Komuro, H. Yamamoto, Y. Utsumi, K. Ohomori, and T. Kozawa, *Appl. Phys. Express*, **6** (2012) 14001.
16. N. Mojarad, J. Gobrecaht, and Y. Ekinci, *Sci. Rep.*, **5** (2015) 9235.
17. P. D. Ashby, D. L. Olynick, D. F. Ogletree, and P. P. Naulleau, *Adv. Mater.*, **27** (2015) 5813.
18. K. D. Closser, D. F. Ogletree, P. Naulleau, and D. Prendergast, *J. Chem. Phys.*, **146** (2017) 164106.
19. S. Grzeskowiak, A. Narasimhan, M. Murphy, C. Ackerman, J. Kaminsky, R. L. Brainard, and G. Denbeaux, *Proc. SPIE*, **10146** (2017) 101462C.
20. J. Haitjema, L. Wu, A. Giuliani, L. Nahon, S. Castellanos, and A. M. Brouwer, *J. Photopolym. Sci. Technol.*, **31** (2018) 243.
21. L. Wu, M. Tiekink, A. Giuliani, L. Nahon, and S. Castellanos, *J. Mater. Chem. C*, **7** (2019) 33.
22. L. Nahon, N. De Oliveira, G. A. Garcia, J. F. Gil, B. Pilette, O. Marcouillé, B. Lagarde, and F. Polack, *J. Synchrotron Radiat.*, **19** (2012) 508.
23. A. R. Milosavljević, C. Nicolas, J. F. Gil, F. Canon, M. Réfrégiers, L. Nahon, and A. Giuliani, *J. Synchrotron Radiat.*, **19** (2012) 174.
24. Gaussian 16, Revision C.01, M. J. Frisch, G. W. Trucks, H. B. Schlegel, G. E. Scuseria, M. A. Robb, J. R. Cheeseman, G. Scalmani, V. Barone, G. A. Petersson, H. Nakatsuji, X. Li, M. Caricato, A. Marenich, J. Bloino, B. G. Janesko, R. Gomperts, B. Mennucci, H. P. Hratchian, J. V. Ortiz, A. F. Izmaylov, J. L. Sonnenberg, D. Williams-Young, F. Ding, F. Lipparini, F. Egidi, J. Goings, B. Peng, A. Petrone, T. Henderson, D. Ranasinghe, V. G. Zakrzewski, J. Gao, N. Rega, G. Zheng, W. Liang, M. Hada, M. Ehara, K. Toyota, R. Fukuda, J. Hasegawa, M. Ishida, T. Nakajima, Y. Honda, O. Kitao, H. Nakai, T. Vreven, K. Throssell, J. A. Montgomery, Jr., J. E. Peralta, F. Ogliaro, M. Bearpark, J. J. Heyd, E. Brothers, K. N. Kudin, V. N. Staroverov, T. Keith, R. Kobayashi, J. Normand, K. Raghavachari, A. Rendell, J. C. Burant, S. S. Iyengar, J. Tomasi, M. Cossi, J. M. Millam, M. Klene, C. Adamo, R. Cammi, J. W. Ochterski, R. L. Martin, K. Morokuma, O. Farkas, J. B. Foresman, and D. J. Fox, Gaussian, Inc., Wallingford CT, 2016.
25. H. Xu, K. Yang, K. Sakai, V. Kosma, K. Kasahara, E. P. Giannelis, and C. K. Ober, *Proc. SPIE*, **10583** (2018) 105831P.
26. L. Patiny and A. Borel, *J. Chem. Inf. Model.,* **53** (2013) 1223.